Journal of Computational Mathematics
Vol.xx, No.x, 2026, 1–23.

http://www.global-sci.org/jcm
doi:10.4208/jcm.2509-m2024-0241

THE QUADRATIC DISCONTINUOUS FINITE VOLUME ELEMENT SCHEMES FOR ELLIPTIC PROBLEMS*

Yuzhi Lou
School of Mathematics and Information Sciences, Yantai University, Yantai 264005, China
Email: 1123097197@qq.com
Hongxing Rui
School of Mathematics, Shandong University, Jinan 250100, China
Email: hxrui@sdu.edu.cn
Xiufang Feng[1)]
School of Mathematics and Statistics, Ningxia University, Yinchuan 750000, China
Email: xf_feng@nxu.edu.cn

Abstract

The objective of the paper is to develop the quadratic discontinuous finite volume methods (DFVM) for solving elliptic equations with variable coefficients. The proposed numerical schemes are composed of the discontinuous Galerkin (DG) method with different interior penalty formulations (IIPG, NIPG, SIPG) and the finite volume element method which the trial function is discontinuous quadratic element function. Subsequently, with the specialized projection techniques, we built up a bridge between the bilinear form of DFVM and that of DG method, which simplifies the analysis and proves the optimal error estimate of the schemes in the broken H^1 norm. Finally, we provide numerical simulations to validate the theoretical findings.

Mathematics subject classification: 65N08, 65N12, 65N15.
Key words: Discontinuous finite volume element method, Quadratic element, Error estimates, Elliptic problems.

1. Introduction

In this paper, we explore the following second-order elliptic boundary value problem:

$$\begin{cases} -\nabla \cdot (B\nabla u) = f & \text{in } \Omega, \\ u(x) = 0 & \text{on } \partial\Omega, \end{cases} \tag{1.1}$$

where Ω is a bounded, convex polygonal domain in R^2 with boundary $\partial\Omega$. The matrix-value function $B = (b_{ij})_{2\times 2} \in W^{1,\infty}(\Omega)^4$ satisfies the uniformly elliptic condition: There exists a constant $\beta > 0$ such that

$$\beta\delta^\top\delta \le \delta^\top B\delta, \quad \forall\, \delta \in R^2.$$

In 1973, Reed and Hill [17] developed the discontinuous Galerkin method for linear hyperbolic problems. Due to its discontinuous nature across internal element boundaries, the DG method offers several advantages, including high accuracy, the ability to handle meshes with hanging nodes, strong parallel computing capabilities, and excellent performance in handling

* Received October 25, 2024 / Revised version received June 27, 2025 / Accepted September 8, 2025 / Published online March 2, 2026 /
[1)] Corresponding author

complex geometries. Consequently, it has attracted numerous scholars to further explore its potential [1–5,12,22]. The finite volume element (FVM) method is a classical numerical method that not only can handle complex geometries, like the finite element method (FEM), but is also favored for its ability to maintain local conservation of mass, momentum, or energy. However, most of the existing finite volume methods for solving partial differential equations are of low order [10, 13, 18, 19, 24, 25, 28]. The theoretical analysis of the higher-order FVM schemes remains challenging due to the dependence of their discrete bilinear form on the region division. However, significant progress has been made in recent years regarding high-order finite volume research. Some researchers [6–9] established the convergence analysis of the higher-order FVM method for elliptic problems under minimum angle conditions based on elementwise stiffness matrix analysis. Additional relevant research advances can be referred to [21, 23, 29].

Noting the significant advantages of DG and FVM, Ye [26] combined the two methods to propose the discontinuous finite volume method in 2004, and applied it to solving elliptic problems, as well as deriving the corresponding error estimates under the mesh-dependent norm. In 2007, literature [11] established a general framework for analyzing the class of finite volume methods that employ continuous or totally discontinuous trial functions and piecewise constant test functions, and derived optimal error estimates in both H^1 and L^2 norms. The discontinuous finite volume method combines some advantages of the finite volume element method and the internally penalized discontinuous Galerkin method, and has the characteristics of conservation, flexibility in mesh refinement, ability to handle complex geometric shapes, and simplicity of implementation. The uniqueness of discontinuous finite volume element lies in the fact that the size of its control body is only half or even smaller than that of the traditional finite volume method. Most importantly, it only involves one triangular element in the primary partition, which has better locality and is conducive to parallel computing. In addition, in some existing DFVM research on time-dependent problems [15], it can be seen that the mass matrix of DFVM is block diagonal, extending the advantage of DG to the finite volume method, which is also an attractive feature. However, the discontinuous finite volume method currently cannot approximate with arbitrary-order polynomials like the DG method, and its construction is indeed more complex than the DG method. The optimal convergence rate of L^2 error is also affected by dual partition and penalty parameter, which is also an area that needs further optimization and research. Some recent developments on the DFVM can be found in [14, 20], but the approximate functions used in these literatures are of low order.

In this paper, we construct the second-order discontinuous finite volume element algorithms with different internal penalty formulations for solving variable coefficient elliptic problems, which incorporate the merits of the classical discontinuous Galerkin method and the finite volume method. With the favorable properties of the special projection, we obtain the continuity and the uniform ellipticity of the bilinear form of the DFVM algorithms, which enables us to obtain corresponding error analysis of the scheme in the broken H^1 norm. Finally, the correctness of the theoretical analysis and the strengths and weaknesses of the proposed algorithm are verified by numerical examples. The proposed DFVM algorithm is not only easy to implement and capable of achieving the desired accuracy, but also has the property of local conservation of physical quantities. Furthermore, the sensitivity of the DFVM algorithm with different internal penalty terms to penalty parameters is consistent with the performance of the corresponding DG scheme, that is, the nonsymmetric interior penalty Galerkin (NIPG) scheme is less sensitive to penalty parameters compared to the incomplete interior penalty Galerkin (IIPG) and symmetric interior penalty Galerkin (SIPG) schemes.

This paper is organized in 6 sections. We introduce dual decomposition, abstract function space, and a novel mapping in Section 2. In Section 3, we propose three DFVM algorithms for elliptic problems and discuss the properties of the bilinear form of the DFVM. In Section 4, we give error estimate for the DFVM schemes. In Section 5, the characteristics of the algorithms are verified by numerical experiments. Finally, conclusions are given in Section 6.

Throughout the paper, the letter C denotes a positive constant independent of the mesh size and may indicate different values in different places.

2. Preliminaries and Notations

Let $\mathcal{T}_h = \{k\}$ denote a regular triangulation of the region Ω, such that $\bar{\Omega} = \cup_{k\in\mathcal{T}_h} k$, and $\mathrm{diam}(k) \le h$. With respect to the trial space U_h, we choose the discontinuous Lagrange quadratic element space associated with the primary partition $\mathcal{T}_h$ as follows:

$$U_h := \left\{u \in L^2(\Omega),\ u|_k \in P_2(k),\ \forall\, k \in \mathcal{T}_h\right\}, \tag{2.1}$$

where $P_n(k)$ represents the space of polynomial functions of degree equal to or less than n over k.

Next, we shall specify the construction of dual partition $\mathcal{T}_h^* = \{k^*\}$ of the primal mesh $\mathcal{T}_h$, whose element is called dual element or control volume. Each control volume k^* is a polygon that corresponds to a vertex or a midpoint of a triangular element. First, for any triangle $k = \triangle A_1A_2A_3 \in \mathcal{T}_h$, we write its barycenter as O, and the midpoints of the edges $\overline{A_2A_3}$, $\overline{A_3A_1}$, $\overline{A_1A_2}$ as m_1, m_2, m_3, respectively. Then, we need to select some dual nodes $q_i, i = 1, 2, 3$ and g_{ij}, $i, j = 1, 2, 3, i \ne j$ on edges $\overline{A_im_i}$ and $\overline{A_iA_j}$, respectively, such that the following relations holds:

$$\frac{|A_ig_{ij}|}{|A_iA_j|} = a, \quad \frac{|A_iq_i|}{|A_im_i|} = b, \tag{2.2}$$

where g_{ij} is required to be closer to A_i than to A_j, and a and b are two mesh parameters.

The control volume $k^*_{A_1}$ of vertex A_1 is constructed by sequentially connecting its surrounding dual nodes $g_{12}, q_1, g_{13}, A_1, g_{12}$, as depicted in red line in Fig. 2.1. Similarly, the control volume $k^*_{m_1}$ of the midpoint m_1 can be obtained by successively connecting its surrounding dual nodes $g_{23}, m_1, g_{32}, q_3, O, q_2, g_{23}$, as indicated by the blue line in Fig. 2.1. The control volumes of the remaining nodes of the triangle $k \in \mathcal{T}_h$ are constructed in a similar way.

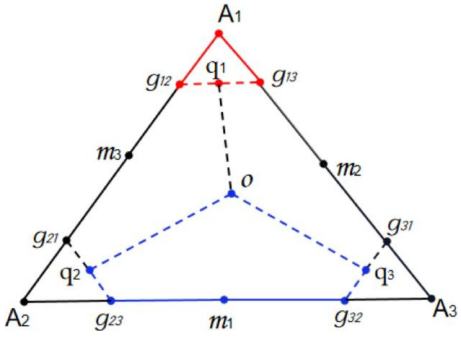

Fig. 2.1. Schematic of a control volume on a triangular element with dual mesh parameters $a = b = (1 - 1/\sqrt{3})/2$.

It is easy to notice that once the values of the dual mesh parameters a and b are changed, different dual partitions will be obtained. The effects and relationships of the dual mesh parameters a and b on the quadratic FVM scheme have been discussed in the literature [7,23]. In this paper, we take the values of the dual mesh parameters a and b both to be $(1-1/\sqrt{3})/2$. And it is not hard to prove

$$|k_{A_i^*}| = \left(\frac{1}{3} - \frac{1}{2\sqrt{3}}\right)|k|, \quad |k_{m_i^*}| = \frac{1}{2\sqrt{3}}|k|. \tag{2.3}$$

The test function space U_h^* is taken to be the piecewise constant function space associated with the dual decomposition $\mathcal{T}_h^*$ as follows:

$$U_h^* = \left\{\xi \in L^2(\Omega) : \xi|_{k^*} \in P_0(k^*),\ \forall\, k^* \in \mathcal{T}_h^*\right\}. \tag{2.4}$$

In this paper, we use the standard notations for the Sobolev spaces $H^k(\Omega) = W^{k,2}(\Omega)$, $(1 \le k \le \infty)$ with the norm $\|\cdot\|_{k,\Omega}$ and seminorm $|\cdot|_{k,\Omega}$. And $\|\cdot\|_e$ is L^2 integration on edge e.

The operation between two matrix-valued variables σ and τ is defined by $\sigma{:}\tau = \sum_{i,j=1}^{2} \sigma_{ij}\tau_{ij}$. Let k_1 and k_2 be two neighboring elements in the triangulation $\mathcal{T}_h$. And $e = \partial k_1 \cap \partial k_2$, $\boldsymbol{n_1} = \boldsymbol{n}|_{\partial k_1}$ and $\boldsymbol{n_2} = \boldsymbol{n}|_{\partial k_2}$ are the exterior unit normal vectors on ∂k_1 and ∂k_2, respectively. In order to deal with the discontinuity of finite element functions crossing the interface of elements, the following average $\{\cdot\}$ and jump $[\cdot]$ on e for scalar q and vector $\boldsymbol{w}$ are defined by

$$\begin{aligned}
\{q\} &= \frac{1}{2}(q|_{\partial k_1} + q|_{\partial k_2}), \qquad [q] = q|_{\partial k_1}\boldsymbol{n_1} + q|_{\partial k_2}\boldsymbol{n_2},\\
\{\boldsymbol{w}\} &= \frac{1}{2}(\boldsymbol{w}|_{\partial k_1} + \boldsymbol{w}|_{\partial k_2}), \quad [\boldsymbol{w}] = \boldsymbol{w}|_{\partial k_1}\cdot\boldsymbol{n_1} + \boldsymbol{w}|_{\partial k_2}\cdot\boldsymbol{n_2}.
\end{aligned}$$

If the edge $e \subset \partial\Omega$, then

$$\{q\} = q, \quad [\boldsymbol{w}] = \boldsymbol{w}\cdot\boldsymbol{n}.$$

Let Γ be the set of edges of all triangles k in $\mathcal{T}_h$ and $\Gamma_0 := \Gamma \setminus \partial\Omega$. After a simple derivation, it is not difficult to obtain the following classic identity equation:

$$\sum_{k\in\mathcal{T}_h}\int_{\partial k} q\boldsymbol{v}\cdot\boldsymbol{n}ds = \sum_{e\in\Gamma}\int_e [q]\cdot\{\boldsymbol{v}\}ds + \sum_{e\in\Gamma_0}\int_e \{q\}[\boldsymbol{v}]ds. \tag{2.5}$$

Let $U(h) = U_h + (H^2(\Omega)\cap H_0^1(\Omega))$. We now introduce a mapping $\gamma : U(h) \to U_h^*$ satisfying

$$\begin{aligned}
&\gamma v|_{k^*_{A_i}} = v(A_i)|_k, && \forall\, v \in U(h),\\
&\gamma v|_{k^*_{m_i}} = \frac{2}{\sqrt{3}}v(m_i)|_k + \frac{1}{2}\left(1 - \frac{2}{\sqrt{3}}\right)\left(v(A_{i+1})|_k + v(A_{i+2})|_k\right), && \forall\, v \in U(h),
\end{aligned}$$

where $A_i, i = 1,2,3$, is vertex of the triangle element $k \in \mathcal{T}_h$ and $m_i, i = 1,2,3$, is the midpoint of the opposite edge of vertex $A_i, i = 1,2,3$. Based on the results of the literature [27, 29], some desirable properties of the above mapping γ are listed below. If the parameters a and b of the dual mesh fulfill $a \in (0, 1/2)$ and $b \in (0, 2/3)$, respectively, then there exist two constants $c > 0, C > 0$ such that

$$c\|w\|_{0,k} \le \|\gamma w\|_{0,k} \le C\|w\|_{0,k}, \quad \forall\, w \in U_h, \qquad \forall\, k \in \mathcal{T}_h, \tag{2.6}$$

$$\|w - \gamma w\|_{0,k} \le Ch_k|w|_{1,k}, \qquad \forall\, w \in U(h), \quad \forall k \in \mathcal{T}_h. \tag{2.7}$$

Suppose k_1 and k_2 are two neighboring elements in $\mathcal{T}_h$ and $e = \partial k_1 \cap \partial k_2$, then

$$\int_e (v - \gamma v)|_k ds = 0, \qquad \forall\, v \in U_h, \tag{2.8}$$

$$\int_e w|_k (v - \gamma v)|_k ds = 0, \quad \forall\, v \in U_h, \quad w \in Q_h, \tag{2.9}$$

where $k = k_1$ or k_2,

$$Q_h := \big\{ v \in L^2(\Omega) : v|_k \in P_1(k),\ \forall\, k \in \mathcal{T}_h \big\}.$$

Note that Eqs. (2.8) and (2.9) also hold for boundary edges $e \in \Gamma \cap \partial\Omega$.

And for all $k \in \mathcal{T}_h$,

$$\int_k (v - \gamma v) dxdy = 0, \quad \forall\, v \in U_h. \tag{2.10}$$

3. Discontinuous Finite Volume Element Scheme

Our central task of this section is to establish the quadratic DFVM schemes for the elliptic problem (1.1) and make the corresponding theoretical analysis for these schemes.

We multiply both sides of the elliptic equation (1.1) by $\xi \in U_h^*$. Then, by integrating the obtained results over the entire region and applying Green's formulation, we can derive

$$-\sum_{k^* \in \mathcal{T}_h^*} \int_{k^*} \nabla \cdot (B\nabla u) \cdot \xi dxdy = -\sum_{k^* \in \mathcal{T}_h^*} \int_{\partial k^*} B\nabla u \cdot \boldsymbol{n} \xi ds = \sum_{k^* \in \mathcal{T}_h^*} \int_{k^*} f\xi dxdy, \tag{3.1}$$

where $\boldsymbol{n}$ is the unit outward normal vector on ∂k^*.

For $\forall k \in \mathcal{T}_h$, the above formulation can be represented as

$$\begin{aligned} &-\sum_{k^* \in \mathcal{T}_h^*} \int_{\partial k^*} B\nabla u \cdot \boldsymbol{n} \xi ds \\ &= -\sum_{k \in \mathcal{T}_h} \Bigg(\sum_{j=1}^{3} \int_{g_{j\,j+1} q_j + q_j g_{j\,j+2}} B\nabla u \cdot \boldsymbol{n} \xi ds \\ &\qquad + \sum_{j=1}^{3} \int_{O q_j + q_j g_{j\,j+1} + g_{j+1\,j} q_{j+1} + q_{j+1} O} B\nabla u \cdot \boldsymbol{n} \xi ds + \int_{\partial k} B\nabla u \cdot \boldsymbol{n} \xi ds \Bigg), \end{aligned}$$

when $j+1 > 3$ or $j+2 > 3$, we take $j+1 = (j+1) \bmod 3$ and $j+2 = (j+2) \bmod 3$.

For the sake of brevity of writing, we set $\partial k^{*,0}$ to be the dual side that is inside the triangle $k \in \mathcal{T}_h$. Then the above formulation can be rewritten as

$$-\sum_{k^* \in \mathcal{T}_h^*} \int_{\partial k^*} B\nabla u \cdot \boldsymbol{n} \xi ds = -\sum_{k \in \mathcal{T}_h} \Bigg(\sum_{k^* \in k} \int_{\partial k^{*,0}} B\nabla u \cdot \boldsymbol{n} \xi ds + \int_{\partial k} B\nabla u \cdot \boldsymbol{n} \xi ds \Bigg). \tag{3.2}$$

By employing the classical relation (2.5) in discontinuous Galerkin method and noting the fact that $[B\nabla u] = 0$ for $u \in H_0^1(\Omega) \cap H^2(\Omega)$ on Γ_0, it can be concluded that

$$-\sum_{k \in \mathcal{T}_h} \int_{\partial k} B\nabla u \cdot \boldsymbol{n} \xi ds = -\sum_{e \in \Gamma} \int_e \{B\nabla u\} \cdot [\xi] ds. \tag{3.3}$$

Substituting (3.2), (3.3) into (3.1), one gets

$$\begin{aligned}
&-\sum_{k^*\in\mathcal{T}_h^*}\int_{\partial k^*} B\nabla u\cdot\boldsymbol{n}\xi ds\\
&=-\sum_{k\in\mathcal{T}_h}\sum_{k^*\in k}\int_{\partial k^{*,0}} B\nabla u\cdot\boldsymbol{n}\xi ds-\sum_{e\in\Gamma}\int_e\{B\nabla u\}\cdot[\xi]ds\\
&=\sum_{k^*\in\mathcal{T}_h^*}\int_{k^*} f\xi dxdy. \qquad (3.4)
\end{aligned}$$

We define the bilinear forms as follows:

$$\begin{aligned}
A_*(u,\xi)&=-\sum_{k\in\mathcal{T}_h}\sum_{k^*\in k}\int_{\partial k^{*,0}} B\nabla u\cdot\boldsymbol{n}\gamma\xi ds,\\
A_1(u,v)&=A_*(u,v)-\sum_{e\in\Gamma}\int_e\{B\nabla u\}\cdot[\gamma v]ds+\alpha\frac{1}{h_e}\sum_{e\in\Gamma}\int_e[\gamma u]\cdot[\gamma v]ds,
\end{aligned}$$

where $\alpha\geq 0$ is the penalty parameter commonly used in the discontinuous Galerkin method and will be specified later.

Since $[\gamma u]=0$, it follows that the exact solution u of the elliptic equations (1.1) satisfies

$$A_1(u,v)=(f,\gamma v),\quad \forall\, v\in U_h. \qquad (3.5)$$

Algorithm 3.1: DFVM-IIPG.

The quadratic discontinuous finite volume scheme with incomplete interior penalty for (1.1) aims to find a solution $u_h\in U_h$ such that

$$A_1(u_h,v)=(f,\gamma v),\quad \forall\, v\in U_h. \qquad (3.6)$$

Next, we establish two other quadratic discontinuous finite volume algorithms based on the internal penalty discontinuous Galerkin formulation. We define

$$A_2(u,v)=A_1(u,v)+\sum_{e\in\Gamma}\int_e\{B\nabla v\}\cdot[\gamma u]ds.$$

Algorithm 3.2: DFVM-NIPG.

The quadratic discontinuous finite volume element method with nonsymmetric interior penalty for (1.1) is to seek $u_h\in U_h$ such that

$$A_2(u_h,v)=(f,\gamma v),\quad \forall\, v\in U_h.$$

And, we define

$$A_3(u,v)=A_1(u,v)-\sum_{e\in\Gamma}\int_e\{B\nabla v\}\cdot[\gamma u]ds.$$

Algorithm 3.3: DFVM-SIPG.

The quadratic discontinuous finite volume element method with symmetric interior penalty for (1.1) is to find $u_h \in U_h$ such that

$$A_3(u_h, v) = (f, \gamma v), \quad \forall\, v \in U_h.$$

Algorithms 3.1-3.3 can be uniformly represented as finding $u_h \in U_h$ such that

$$A(u_h, v) = (f, \gamma v), \quad \forall\, v \in U_h, \tag{3.7}$$

where

$$A(u, v) = A_1(u, v) + \theta \sum_{e\in\Gamma} \int_e \{B\nabla v\} \cdot [\gamma u] ds,$$

and $\theta = -1, 0$ and 1 lead to the Algorithms 3.3, 3.1 and 3.2, respectively.

Let $\nabla_h v$ be the functions whose restriction to each element $k \in \mathcal{T}_h$ are equal to ∇v.

The specific definition of the norm for the space $U(h)$ is as follows:

$$|||v|||_1^2 = |v|_{1,h}^2 + \sum_{e\in\Gamma} \frac{1}{h_e} \int_e [\gamma v]_e^2 ds,$$
$$|||v|||^2 = |||v|||_1^2 + \sum_{k\in\mathcal{T}_h} h_k^2 |v|_{2,k}^2,$$

where

$$|v|_{1,h}^2 = \sum_{k\in\mathcal{T}_h} |v|_{1,k}^2.$$

From the standard inverse inequality, it can be discovered that $|||\cdot|||$ and $|||\cdot|||_1$ are equivalent.

We recall the following trace theorem (see [2]). Let k be a triangular element and let e denote one of its edges. The theorem states that there exists a constant $C_1, C_2 > 0$ such that for any function $g \in H^2(k)$,

$$\|g\|_e^2 \le C_1\big(h_k^{-1}\|g\|_k^2 + h_k |g|_{1,k}^2\big), \tag{3.8}$$
$$\left\|\frac{\partial g}{\partial \boldsymbol{n}}\right\|_e^2 \le C_2\big(h_k^{-1}|g|_{1,k}^2 + h_k |g|_{2,k}^2\big), \tag{3.9}$$

where C_1, C_2 are associated only with the minimum angle of element k.

Lemma 3.1. *For any $u, v \in U(h)$, we have*

$$A_*(u, v) = (B\nabla_h u, \nabla_h v) + \sum_{k\in\mathcal{T}_h} \int_{\partial_k} (\gamma v - v) B\nabla u \cdot \boldsymbol{n} ds + \sum_{k\in\mathcal{T}_h} (\nabla \cdot B\nabla u, v - \gamma v)_k. \tag{3.10}$$

Furthermore, if $u, v \in U_h$, then

$$A_*(u, v) \ge (B\nabla_h u, \nabla_h v) - C^* h |||u||| \, |||v|||. \tag{3.11}$$

Proof. First, note that after applying the projection operator γ, the $\gamma \boldsymbol{v}$ is a constant on each control volume. Then we apply the divergence theorem on each control volume, followed by the Green's formula, which allows us to derive

$$\begin{aligned}
A_*(u,v) &= \sum_{k\in\mathcal{T}_h}\sum_{j=1}^{3}\int_{A_jA_{j+1}} B\nabla u\cdot\boldsymbol{n}\gamma v ds - \sum_{k\in\mathcal{T}_h}\sum_{k^*\in k}\int_{\partial k^*} B\nabla u\cdot\boldsymbol{n}\gamma v ds\\
&= \sum_{k\in\mathcal{T}_h}\sum_{j=1}^{3}\int_{A_jA_{j+1}} B\nabla u\cdot\boldsymbol{n}\gamma v ds - \sum_{k\in\mathcal{T}_h}\sum_{k^*\in k}\int_{k^*} \nabla\cdot(B\nabla u)\gamma v dxdy\\
&= \sum_{k\in\mathcal{T}_h}\int_{\partial k} B\nabla u\cdot\boldsymbol{n}(\gamma v - v)ds + \sum_{k\in\mathcal{T}_h}\int_{\partial k} B\nabla u\cdot\boldsymbol{n} v ds - \sum_{k\in\mathcal{T}_h}\big(\nabla\cdot(B\nabla u),\gamma v\big)_k\\
&= \sum_{k\in\mathcal{T}_h}\int_{\partial k} B\nabla u\cdot\boldsymbol{n}(\gamma v - v)ds + \sum_{k\in\mathcal{T}_h}(B\nabla u,\nabla v)_k + \sum_{k\in\mathcal{T}_h}\big(\nabla\cdot(B\nabla u), v-\gamma v\big)_k\\
&= (B\nabla_h u,\nabla_h v) + \sum_{k\in\mathcal{T}_h}\int_{\partial k} B\nabla u\cdot\boldsymbol{n}(\gamma v - v)ds + \sum_{k\in\mathcal{T}_h}\big(\nabla\cdot(B\nabla u), v-\gamma v\big)_k\\
&=: \sum_{i=1}^{3} T_i. \qquad (3.12)
\end{aligned}$$

If $u, v \in U_h$, and assuming that $\widetilde{B}$ denotes the function value of B at the midpoint of the side of the triangle, with the help of the trace inequality and Hölder inequality, we get

$$\begin{aligned}
T_2 &= \sum_{k\in\mathcal{T}_h}\int_{\partial k}(B-\widetilde{B})\nabla u\cdot\boldsymbol{n}(\gamma v - v)ds\\
&\le \sum_{k\in\mathcal{T}_h}\|B-\widetilde{B}\|_{L^\infty(\partial k)}\int_{\partial k}\nabla u\cdot\boldsymbol{n}(\gamma v - v)ds\\
&\le \sum_{k\in\mathcal{T}_h}\|B-\widetilde{B}\|_{L^\infty(k)}\int_{\partial k}\nabla u\cdot\boldsymbol{n}(\gamma v - v)ds\\
&\le \sum_{k\in\mathcal{T}_h} Ch\|B\|_{1,\infty}\|\gamma v - v\|_{L^2(\partial k)}\|\nabla u\cdot\boldsymbol{n}\|_{L^2(\partial k)}.
\end{aligned}$$

Thanks to inequalities (3.8) and (3.9) and the operator property (2.7), we arrive at

$$\begin{aligned}
T_2 &\le Ch\|B\|_{1,\infty}\left(\sum_{k\in\mathcal{T}_h}\big(h_k^{-1}\|\gamma v - v\|_k^2 + h_k|\gamma v - v|_{1,k}^2\big)\right)^{\frac{1}{2}}\\
&\quad\times\left(\sum_{k\in\mathcal{T}_h}\big(h_k^{-1}\|\nabla u\|_k^2 + h_k|\nabla u|_{1,k}^2\big)\right)^{\frac{1}{2}}\\
&\le Ch\|B\|_{1,\infty}\left(\sum_{k\in\mathcal{T}_h} h_k|v|_{1,k}^2\right)^{\frac{1}{2}}\left(\sum_{k\in\mathcal{T}_h}\big(h_k^{-1}|u|_{1,k}^2 + h_k|u|_{2,k}^2\big)\right)^{\frac{1}{2}}\\
&\le Ch\|B\|_{1,\infty}\left(\sum_{k\in\mathcal{T}_h}|v|_{1,k}^2\right)^{\frac{1}{2}}\left(\sum_{k\in\mathcal{T}_h}\big(|u|_{1,k}^2 + h_k^2|u|_{2,k}^2\big)\right)^{\frac{1}{2}} \le Ch|||v|||\,|||u|||. \qquad (3.13)
\end{aligned}$$

As for T_3 term, we have

$$T_3 = \sum_{k\in\mathcal{T}_h} (\nabla B\cdot\nabla u, v-\gamma v)_k + \sum_{k\in\mathcal{T}_h} \big(B\nabla\cdot(\nabla u), v-\gamma v\big)_k =: T_{31}+T_{32}. \tag{3.14}$$

For the first term of T_3, we once again apply the Hölder inequality and property (2.7), we can reach

$$\begin{aligned}
|T_{31}| &\le C\sum_{k\in\mathcal{T}_h} \|\nabla B\|_{L^\infty(k)}\|\nabla u\|_{L^2(k)}\|v-\gamma v\|_{L^2(k)}\\
&\le C\|B\|_{1,\infty}\left(\sum_{k\in\mathcal{T}_h}|u|_{1,k}^2\right)^{\frac12}\left(\sum_{k\in\mathcal{T}_h}h^2|v|_{1,k}^2\right)^{\frac12}\\
&\le C_3 h\|B\|_{1,\infty}|||u|||\,|||v|||.
\end{aligned} \tag{3.15}$$

As for the second term T_{32}, it is assumed that B^* is the function value of B at the barycenter of the triangle element. Similar to the proof of T_2, it holds that

$$\begin{aligned}
T_{32} &= \sum_{k\in\mathcal{T}_h}(B-B^*)\big(\nabla\cdot(\nabla u), v-\gamma v\big)_k\\
&\le C\sum_{k\in\mathcal{T}_h}\|B-B^*\|_{L^\infty(k)}\|\nabla\cdot(\nabla u)\|_{L^2(k)}\|v-\gamma v\|_{L^2(k)}\\
&\le Ch\|B\|_{1,\infty}\left(\sum_{k\in\mathcal{T}_h}|u|_{2,k}^2\right)^{\frac12}\left(\sum_{k\in\mathcal{T}_h}h_k^2|v|_{1,k}^2\right)^{\frac12}\\
&\le Ch\|B\|_{1,\infty}\left(\sum_{k\in\mathcal{T}_h}h_k^2|u|_{2,k}^2\right)^{\frac12}\left(\sum_{k\in\mathcal{T}_h}|v|_{1,k}^2\right)^{\frac12}\\
&\le C_4 h\|B\|_{1,\infty}|||u|||\,|||v|||.
\end{aligned} \tag{3.16}$$

Thus, combining (3.13),(3.15) and (3.16), if $u, v\in U_h$, we get

$$A_*(u,v)\ge (B\nabla_h u,\nabla_h v) - C^*h|||u|||\,|||v|||.$$

The proof is complete. □

Lemma 3.2. *$\forall u, v\in U(h)$, there exists a positive constant C such that*

$$A(u,v)\le C|||u|||\,|||v|||. \tag{3.17}$$

Proof. It follows from Lemma 3.1, we can derive

$$\begin{aligned}
|A_*(u,v)| &\le |(B\nabla_h u,\nabla_h v)| + \left|\sum_{k\in\mathcal{T}_h}\int_{\partial_k}(\gamma v - v)B\nabla u\cdot\boldsymbol{n}ds\right| + \left|\sum_{k\in\mathcal{T}_h}(\nabla\cdot B\nabla u, v-\gamma v)_k\right|\\
&\le C\Bigg(|u|_{1,h}|v|_{1,h} + \left(\sum_{k\in\mathcal{T}_h}|v|_{1,k}^2\right)^{\frac12}\left(\sum_{k\in\mathcal{T}_h}\big(|u|_{1,k}^2+h^2|u|_{2,k}^2\big)\right)^{\frac12}\\
&\quad + \left(\sum_{k\in\mathcal{T}_h}|u|_{1,k}^2\right)^{\frac12}\left(\sum_{k\in\mathcal{T}_h}h^2|v|_{1,k}^2\right)^{\frac12}\Bigg) \le C|||u|||\,|||v|||.
\end{aligned} \tag{3.18}$$

Next, we prove the boundedness of the remaining terms of the bilinear form $A(u,v)$

$$\begin{aligned}
&\left| -\sum_{e\in\Gamma}\int_e \{B\nabla u\}\cdot[\gamma v]ds \right| \\
&\le C\sum_{e\in\Gamma}\left(\int_e h_e\{B\nabla u\}^2 ds\right)^{\frac{1}{2}}\left(\int_e h_e^{-1}[\gamma v]^2 ds\right)^{\frac{1}{2}} \\
&\le \left(\sum_{k\in\mathcal{T}_h}\left(\|B\nabla u\|_{0,k}^2 + h_k^2|B\nabla u|_{1,k}^2\right)\right)^{\frac{1}{2}}\left(\sum_{e\in\Gamma}\int_e h_e^{-1}[\gamma v]^2 ds\right)^{\frac{1}{2}} \\
&\le C\left(\sum_{k\in\mathcal{T}_h}\left(\|B\|_{L^2(k)}^2|u|_{1,k}^2 + h_k^2|B|_{1,k}^2|u|_{2,k}^2\right)\right)^{\frac{1}{2}}|||v|||_1 \\
&\le C\left(|u|_{1,h}^2 + \sum_{k\in\mathcal{T}_h} h_k^2|u|_{2,k}^2\right)^{\frac{1}{2}}|||v|||_1 \le C|||u|||\,|||v|||. \qquad (3.19)
\end{aligned}$$

Similarly, it can be obtained that

$$\left|\theta\sum_{e\in\Gamma}\int_e\{B\nabla v\}\cdot[\gamma u]ds\right| \le C|||u|||\,|||v|||. \qquad (3.20)$$

For the penalty terms, one derives

$$\begin{aligned}
&\alpha\frac{1}{h_e}\sum_{e\in\Gamma}\int_e [\gamma u]|_e : [\gamma v]|_e ds \\
&\le C\alpha\left(\sum_{e\in\Gamma}\int_e \frac{1}{h_e}[\gamma u]_e^2 ds\right)^{\frac{1}{2}}\left(\sum_{e\in\Gamma}\int_e \frac{1}{h_e}[\gamma v]_e^2 ds\right)^{\frac{1}{2}} \\
&\le C|||u|||\,|||v|||. \qquad (3.21)
\end{aligned}$$

Together with (3.18)-(3.21), one can conclude that

$$\begin{aligned}
A(u,v) &= A_*(u,v) - \sum_{e\in\Gamma}\int_e\{B\nabla u\}\cdot[\gamma v]ds \\
&\quad + \theta\sum_{e\in\Gamma}\int_e\{B\nabla v\}\cdot[\gamma u]ds + \alpha\frac{1}{h_e}\sum_{e\in\Gamma}\int_e[\gamma u]\cdot[\gamma v]ds \\
&\le C|||u|||\,|||v|||.
\end{aligned}$$

The proof is complete. □

Now, we discuss the coercivity of the bilinear form $A(\cdot,\cdot)$ with respect to the norm $|||\cdot|||$.

Lemma 3.3. *$\forall\, v \in U_h$, there is a constant C such that when α large enough and h small enough, the uniform ellipticity*

$$A(v,v) \ge C|||v|||^2 \qquad (3.22)$$

holds true.

Proof. According to the conclusion of Lemma 3.1, inequality (3.19), Hölder inequality, ϵ-inequality as well as the trace inequality (3.8) and the inverse inequality, we deduce that

$$\begin{aligned}
A(v,v) &= A_*(v,v) - \sum_{e\in\Gamma}\int_e \{B\nabla v\}\cdot[\gamma v]ds \\
&\quad + \alpha\sum_{e\in\Gamma}\frac{1}{h_e}\int_e [\gamma v]|_e^2 ds + \theta\sum_{e\in\Gamma}\int_e \{B\nabla v\}\cdot[\gamma v]ds \\
&\geq C_1|v|_{1,h}^2 - C^*h|||v|||^2 + \alpha\frac{1}{h_e}\sum_{e\in\Gamma}\int_e [\gamma v]|_e^2 ds \\
&\quad - \frac{(1-\theta)^2}{2\epsilon}\left(\sum_{e\in\Gamma}\int_e h_e\{B\nabla v\}^2 ds\right) - \frac{\epsilon}{2}\left(\sum_{e\in\Gamma}\int_e h_e^{-1}[\gamma v]^2 ds\right) \\
&\geq C_1|v|_{1,h}^2 + \left(\alpha - \frac{\epsilon}{2}\right)\left(\sum_{e\in\Gamma}\int_e h_e^{-1}[\gamma v]^2 ds\right) \\
&\quad - \frac{C_2(1-\theta)^2}{2\epsilon}\left(\sum_{k\in\mathcal{T}_h}\left(|v|_{1,k}^2 + h_k^2|v|_{2,k}^2\right)\right) - C^*h|||v|||^2 \\
&\geq \left(C_1 - \frac{C_2^*(1-\theta)^2}{2\epsilon}\right)|v|_{1,h}^2 + \left(\alpha - \frac{\epsilon}{2}\right)\left(\sum_{e\in\Gamma}\int_e h_e^{-1}[\gamma v]^2 ds\right) - C^*h|||v|||^2. \qquad (3.23)
\end{aligned}$$

For the aforementioned inequality relation, in order to ensure that

$$\left(C_1 - \frac{C_2^*(1-\theta)^2}{2\epsilon}\right)|v|_{1,h}^2 - C^*h|||v|||^2 \geq 0, \qquad (3.24)$$

we must take $\epsilon > 0$ large enough and h small enough. In addition, the penalty parameter α is required to be sufficiently large relative to ϵ. □

4. Error Analysis

The main goal of this section is to give the broken H^1 optimal error estimate for the numerical solution of three DFVM schemes proposed in this paper.

Define Lagrange interpolation operator π_k^1 from $H^3(k)$ to $P_2(k)$, it was proved in [27] that

$$\left\|u - \pi_k^1 u\right\|_{s,k} \leq Ch^{3-s}|u|_{3,k}, \quad \forall\, u \in H^3(k), \quad s = 1,2,3. \qquad (4.1)$$

Similar to reference [16], we define $\Pi_1 : H_0^1(\Omega)\cap H^3(\Omega) \to U_h$ by

$$\Pi_1 u|_k = \pi_k^1 u, \quad \forall\, u \in H_0^1(\Omega)\cap H^3(\Omega), \quad \forall\, k \in \mathcal{T}_h. \qquad (4.2)$$

Based on the definition of the norm $|||\cdot|||$ and (4.1), we obtain

$$\begin{aligned}
|||u - \Pi_1 u|||^2 &= |u - \Pi_1 u|_{1,h}^2 + \sum_{e\in\Gamma}\frac{1}{h_e}\int_e [|\gamma(u - \Pi_1 u)|]_e^2 ds + \sum_{k\in\mathcal{T}_h} h_k^2|u - \Pi_1 u|_{2,k}^2 \\
&\leq C\sum_{k\in\mathcal{T}_h} h_k^4|u|_{3,k}^2 + \sum_{e\in\Gamma}\frac{1}{h_e}\int_e [|\gamma(u - \Pi_1 u)|]_e^2 ds.
\end{aligned}$$

Since Lagrange interpolation keeps node values unchanged, we can get $[|\gamma(u - \Pi_1 u)|] = 0$.

Thus,

$$|||u - \Pi_1 u|||^2 \leq C \sum_{k \in \mathcal{T}_h} h_k^4 |u|_{3,k}^2, \quad \forall\, u \in H_0^1(\Omega) \cap H^3(\Omega). \tag{4.3}$$

Theorem 4.1. *Let u be the exact solution of (1.1) satisfies $u \in H_0^1(\Omega) \cap H^3(\Omega)$ and $u_h \in U_h$ be the solution of the quadratic DFVM scheme (3.7). If triangulation $\mathcal{T}_h$ is quasi-uniform, then there exists a constant $C > 0$, which is independent of h such that*

$$|||u - u_h||| \leq Ch^2 \|u\|_3. \tag{4.4}$$

Proof. Subtracting (3.6) from (3.5), we can obtain

$$A(u - u_h, v) = 0, \quad \forall\, v \in U_h. \tag{4.5}$$

Choosing $v = u_h - \Pi_1 u$ in (4.5), one can deduce

$$\begin{aligned} A(u_h - \Pi_1 u, u_h - \Pi_1 u) &= A_1(u_h - u + u - \Pi_1 u, u_h - \Pi_1 u) \\ &= A(u - \Pi_1 u, u_h - \Pi_1 u). \end{aligned} \tag{4.6}$$

With the help of the (3.17) in Lemma 3.2, we arrive at

$$|A(u_h - \Pi_1 u, u_h - \Pi_1 u)| \leq C|||u - \Pi_1 u||| \, |||u_h - \Pi_1 u|||. \tag{4.7}$$

According to the coercive property of $A(\cdot, \cdot)$, equality (4.6), inequality (4.7) and the interpolation estimate (4.3) that

$$\begin{aligned} \widetilde{C}|||u_h - \Pi_1 u|||^2 &\leq A_1(u_h - \Pi_1 u, u_h - \Pi_1 u) \\ &\leq C|||u - \Pi_1 u||| \, |||u_h - \Pi_1 u||| \\ &\leq Ch^2 \|u\|_3 |||u_h - \Pi_1 u|||. \end{aligned} \tag{4.8}$$

Finally, utilizing the triangle inequality enables us to obtain the desired estimation

$$|||u - u_h||| \leq |||u - \Pi_1 u||| + |||u_h - \Pi_1 u||| \leq Ch^2 \|u\|_3.$$

The proof is complete. □

5. Numerical Experiments

In this section, we will explore the validity and practicability of the quadratic discontinuous finite volume method for elliptic problems described above by using two concrete numerical examples.

Example 5.1. Consider the problem (1.1) with $\Omega = [0, 1] \times [0, 1], B = 1$, and the function f is chosen such that the smooth exact solution is given below

$$u = \exp(x + y).$$

We present in Tables 5.1-5.3 the errors as well as the convergence rates of the quadratic discontinuous finite volume element Algorithm 1 with incomplete internal penalty terms (DFVM-IIPG) for solving the elliptic problem under different penalty parameters, respectively. Observing the data in these tables, it is obvious that for the three selected penalty parameters, the

Table 5.1: Errors and convergence rates of Algorithm 1 (IIPG) with dual partition parameters $a = b = (1 - 1/\sqrt{3})/2$ for Example 5.1.

h	$\|u - u_h\|_0$	Rate	$\|\|\|u - u_h\|\|\|$	Rate	α
1/4	2.7574E-04		1.6300E-01		16
1/8	3.8555E-05	2.84	4.0700E-02	2.00	64
1/16	5.2417E-06	2.88	1.0200E-02	2.00	256
1/32	7.4646E-07	2.81	2.5000E-03	2.03	1024
1/64	1.2657E-07	2.56	6.3766E-04	1.97	4096

Table 5.2: Errors and convergence rates of Algorithm 1 (IIPG) with dual partition parameters $a = b = (1 - 1/\sqrt{3})/2$ for Example 5.1.

h	$\|u - u_h\|_0$	Rate	$\|\|\|u - u_h\|\|\|$	Rate	α
1/4	3.1076E-04		1.6320E-01		10
1/8	6.5020E-05	2.26	4.0300E-02	2.02	10
1/16	1.5854E-05	2.04	1.0000E-02	2.01	10
1/32	3.9803E-06	1.99	2.5000E-03	2.00	10
1/64	1.0006E-06	1.99	6.1942E-04	2.01	10

Table 5.3: Errors and convergence rates of Algorithm 1 (IIPG) with dual partition parameters $a = b = (1 - 1/\sqrt{3})/2$ for Example 5.1.

h	$\|u - u_h\|_0$	Rate	$\|\|\|u - u_h\|\|\|$	Rate	α
1/4	6.2000E-03		2.7710E-01		0.5
1/8	1.3000E-03	2.25	5.9400E-02	2.22	0.5
1/16	3.0010E-04	2.11	1.3200E-02	2.17	0.5
1/32	7.3100E-05	2.04	3.1000E-03	2.09	0.5
1/64	1.8113E-05	2.01	7.2978E-04	2.09	0.5

Table 5.4: Errors and convergence rates of Algorithm 3.1 (IIPG) with dual partition parameters $a = (1 - 1/\sqrt{3})/2, b = (6 + \sqrt{3} - \sqrt{21 + 6\sqrt{3}})/9$ for Example 5.1.

h	$\|u - u_h\|_0$	Rate	$\|\|\|u - u_h\|\|\|$	Rate	α
1/4	2.6323E-04		1.6270E-01		16
1/8	3.6608E-05	2.85	4.0600E-02	2.00	64
1/16	4.8246E-06	2.92	1.0200E-02	1.99	256
1/32	6.1239E-07	2.98	2.5000E-03	2.03	1024
1/64	7.6848E-08	2.99	6.3765E-04	1.97	4096

Table 5.5: Errors and convergence rates of Algorithm 3.1 (IIPG) with dual partition parameters $a = (1 - 1/\sqrt{3})/2, b = (6 + \sqrt{3} - \sqrt{21 + 6\sqrt{3}})/9$ for Example 5.1.

h	$\|u - u_h\|_0$	Rate	$\|\|\|u - u_h\|\|\|$	Rate	α
1/4	2.9361E-04		1.6280E-01		10
1/8	5.9448E-05	2.30	4.0100E-02	2.02	10
1/16	1.4411E-05	2.04	9.9000E-03	2.02	10
1/32	3.6220E-06	1.99	2.5000E-03	1.99	10
1/64	9.1178E-07	1.99	6.1683E-04	2.02	10

error estimates in the broken H^1 norm for the numerical solutions all reach the second order accuracy, which is consistent with the conclusion of Theorem 4.1. In addition, it is also evident that when solving the elliptic problem on the dual partition constructed by the current dual parameters, the L^2 error order of the discontinuous finite volume solution is less than third order, which is the same as the conclusion of the corresponding continuous quadratic FVM scheme.

Tables 5.6-5.8 and Tables 5.11-5.12 respectively provide numerical results for solving the elliptic problem utilizing quadratic discontinuous finite volume element Algorithms 3.2 and 3.3

Table 5.6: Errors and convergence rates of Algorithm 3.2 (NIPG) with dual partition parameters $a = b = (1 - 1/\sqrt{3})/2$ for Example 5.1.

h	$\|u - u_h\|_0$	Rate	$\|\|\|u - u_h\|\|\|$	Rate	α
1/4	1.3000E-03		1.5530E-01		0.1
1/8	2.6958E-04	2.27	3.6500E-02	2.09	0.1
1/16	6.0318E-05	2.16	8.8000E-03	2.05	0.1
1/32	1.4282E-05	2.08	2.1000E-03	2.07	0.1
1/64	3.4770E-06	2.04	5.3011E-04	1.99	0.1

Table 5.7: Errors and convergence rates of Algorithm 3.2 (NIPG) with dual partition parameters $a = b = (1 - 1/\sqrt{3})/2$ for Example 5.1.

h	$\|u - u_h\|_0$	Rate	$\|\|\|u - u_h\|\|\|$	Rate	α
1/4	1.4000E-03		1.5650E-01		0.001
1/8	2.7953E-04	2.32	3.6700E-02	2.09	0.001
1/16	6.2315E-05	2.17	8.8000E-03	2.06	0.001
1/32	1.4706E-05	2.08	2.1000E-03	2.07	0.001
1/64	3.5736E-06	2.04	5.3050E-04	1.99	0.001

Table 5.8: Errors and convergence rates of Algorithm 3.2 (NIPG) with dual partition parameters $a = b = (1 - 1/\sqrt{3})/2$ for Example 5.1.

h	$\|u - u_h\|_0$	Rate	$\|\|\|u - u_h\|\|\|$	Rate	α
1/4	3.9976E-04		1.5860E-01		10
1/8	8.7353E-05	2.19	3.8900E-02	2.03	10
1/16	2.1339E-05	2.03	9.6000E-03	2.02	10
1/32	5.3371E-06	2.00	2.4000E-03	2.00	10
1/64	1.3381E-06	2.00	5.9415E-04	2.01	10

Table 5.9: Errors and convergence rates of Algorithm 3.2 (NIPG) with dual partition parameters $a = (1 - 1/\sqrt{3})/2, b = (6 + \sqrt{3} - \sqrt{21 + 6\sqrt{3}})/9$ for Example 5.1.

h	$\|u - u_h\|_0$	Rate	$\|\|\|u - u_h\|\|\|$	Rate	α
1/4	3.2004E-04		1.6040E-01		16
1/8	3.9238E-05	3.03	4.0600E-02	1.98	64
1/16	4.9206E-06	3.00	1.0200E-02	1.99	256
1/32	6.1561E-07	3.00	2.5000E-03	2.03	1024
1/64	7.6941E-08	3.00	6.3765E-04	1.97	4096

Table 5.10: Errors and convergence rates of Algorithm 3.2 (NIPG) with dual partition parameters $a = (1 - 1/\sqrt{3})/2, b = (6 + \sqrt{3} - \sqrt{21 + 6\sqrt{3}})/9$ for Example 5.1.

h	$\|u - u_h\|_0$	Rate	$\|\|\|u - u_h\|\|\|$	Rate	α
1/4	3.8046E-04		1.5820E-01		10
1/8	8.1749E-05	2.22	3.8800E-02	2.03	10
1/16	1.9961E-05	2.03	9.6000E-03	2.01	10
1/32	5.0037E-06	2.00	2.4000E-03	2.00	10
1/64	1.2566E-06	1.99	5.9158E-04	2.02	10

Table 5.11: Errors and convergence rates of Algorithm 3.3 (SIPG) with dual partition parameters $a = b = (1 - 1/\sqrt{3})/2$ for Example 5.1.

h	$\|u - u_h\|_0$	Rate	$\|\|\|u - u_h\|\|\|$	Rate	α
1/4	1.8529E-04		1.7380E-01		10
1/8	2.2793E-05	3.02	4.3400E-02	2.00	10
1/16	3.7191E-06	2.62	1.0800E-02	2.01	10
1/32	7.8748E-07	2.24	2.7000E-03	2.00	10
1/64	1.8730E-07	2.07	6.7746E-04	1.99	10

Table 5.12: Errors and convergence rates of Algorithm 3.3 (SIPG) with dual partition parameters $a = b = (1 - 1/\sqrt{3})/2$ for Example 5.1.

h	$\|u - u_h\|_0$	Rate	$\|\|\|u - u_h\|\|\|$	Rate	α
1/4	2.1851E-04		1.6650E-01		16
1/8	3.6165E-05	2.60	4.0700E-02	2.03	64
1/16	5.0444E-06	2.84	1.0200E-02	2.00	256
1/32	7.2670E-07	2.80	2.5000E-03	2.03	1024
1/64	1.2478E-07	2.54	6.3766E-04	1.97	4096

Table 5.13: Errors and convergence rates of Algorithm 3.3 (SIPG) with dual partition parameters $a = (1 - 1/\sqrt{3})/2, b = (6 + \sqrt{3} - \sqrt{21 + 6\sqrt{3}})/9$ for Example 5.1.

h	$\|u - u_h\|_0$	Rate	$\|\|\|u - u_h\|\|\|$	Rate	α
1/4	1.8061E-04		1.7350E-01		10
1/8	2.0179E-05	3.16	4.3300E-02	2.00	10
1/16	2.5813E-06	2.97	1.0800E-02	2.00	10
1/32	4.1610E-07	2.63	2.7000E-03	2.00	10
1/64	8.5464E-08	2.28	6.7546E-04	2.00	10

Table 5.14: Errors and convergence rates of Algorithm 3.3 (SIPG) with dual partition parameters $a = (1 - 1/\sqrt{3})/2, b = (6 + \sqrt{3} - \sqrt{21 + 6\sqrt{3}})/9$ for Example 5.1.

h	$\|u - u_h\|_0$	Rate	$\|\|\|u - u_h\|\|\|$	Rate	α
1/4	2.1480E-04		1.6620E-01		16
1/8	3.5503E-05	2.60	4.0700E-02	2.03	64
1/16	4.7910E-06	2.89	1.0200E-02	2.00	256
1/32	6.1131E-07	2.97	2.5000E-03	2.03	1024
1/64	7.6826E-08	2.99	6.3765E-04	1.97	4096

Table 5.15: Errors and convergence rates of Algorithm 3.3 (SIPG) with dual partition parameters $a = (1 - 1/\sqrt{3})/2, b = (6 + \sqrt{3} - \sqrt{21 + 6\sqrt{3}})/9$ for Example 5.1.

h	$\|u - u_h\|_0$	Rate	$\|\|\|u - u_h\|\|\|$	Rate	α
1/4	3.0171E-04		1.6320E-01		120
1/8	3.8374E-05	2.98	4.0800E-02	2.00	240
1/16	4.8543E-06	2.98	1.0200E-02	2.00	480
1/32	6.1102E-07	2.99	2.5000E-03	2.03	960
1/64	7.6664E-08	2.99	6.3757E-04	1.97	1920

with different penalty parameters. The computational results show that the $|||u - u_h|||$ of Algorithms 3.2 and 3.3 have the same second-order convergence rate as that of Algorithm 3.1, which is consistent with the results of the theoretical analysis. In addition, the L^2 error estimates of the numerical solutions obtained by Algorithms 3.2 and 3.3 with the current dual parameters also failed to reach the optimal order, which is the identical to that of Algorithm 3.1. We also investigated the sensitivity of the three algorithms with respect to the penalty parameter. The calculations in Tables 5.6-5.8 show that even if the penalty parameter is quite small, the convergence rate of the numerical solution in the NIPG scheme is not affected, which also matches the results of the corresponding discontinuous finite element method, i.e., the NIPG scheme is insensitive to the penalty parameter. This also reveals that the discontinuous FVM method not only maintains the same accuracy as the discontinuous FEM method, but also has the feature of local conservation.

Example 5.2. Let the calculation area be $\Omega = [-1, 1] \times [-1, 1]$, and the coefficient $B = 1$. We choose the source term f for the elliptic problem (1.1), such that it has the exact solution as follows:

$$u = \cos\left(\frac{\pi x}{2}\right) \cos\left(\frac{\pi y}{2}\right).$$

Tables 5.16-5.18, Tables 5.21-5.23 and Tables 5.26-5.27 present the calculation results of solving elliptic equation of the three DFVM constructed in this paper. The numerical results show that the broken H^1 error estimate of the numerical solutions of the three schemes (DFVM-IIPG, DFVM-NIPG, and DFVM-SIPG) can achieve the expected accuracy under different penalty parameters. In addition, when $\alpha = 0.1$ and $\alpha = 0.001$, the calculation accuracy of $|||u - u_h|||$ obtained by the NIPG scheme is on the same order of magnitude as that of $|||u - u_h|||$ obtained by $\alpha = 10$, and both attain second-order accuracy, which once again verifies the insensitivity of the NIPG scheme to the penalty parameter. This demonstrates that the DFVM

Table 5.16: Errors and convergence rates of Algorithm 3.1 (IIPG) with dual partition parameters $a = b = (1 - 1/\sqrt{3})/2$ for Example 5.2.

h	$\|u - u_h\|_0$	Rate	$\|\|\|u - u_h\|\|\|$	Rate	α
1/4	2.5000E-03		1.4700E-01		16
1/8	2.9828E-04	3.07	3.7400E-02	1.97	64
1/16	4.5894E-05	2.70	9.4000E-03	1.99	256
1/32	9.1117E-06	2.33	2.4000E-03	1.97	1024
1/64	2.1093E-06	2.11	5.9058E-04	2.02	4096

Table 5.17: Errors and convergence rates of Algorithm 3.1 (IIPG) with dual partition parameters $a = b = (1 - 1/\sqrt{3})/2$ for Example 5.2.

h	$\|u - u_h\|_0$	Rate	$\|\|\|u - u_h\|\|\|$	Rate	α
1/4	3.2000E-03		1.4560E-01		10
1/8	7.9872E-04	2.00	3.6300E-02	2.00	10
1/16	2.0348E-04	1.97	9.0000E-03	2.01	10
1/32	5.1564E-05	1.98	2.3000E-03	1.97	10
1/64	1.2990E-05	1.99	5.6312E-04	2.03	10

Table 5.18: Errors and convergence rates of Algorithm 3.1 (IIPG) with dual partition parameters $a = b = (1 - 1/\sqrt{3})/2$ for Example 5.2.

h	$\|u - u_h\|_0$	Rate	$\|\|\|u - u_h\|\|\|$	Rate	α
1/4	4.4400E-02		1.7190E-01		0.5
1/8	1.1800E-02	1.91	4.1400E-02	2.05	0.5
1/16	3.0000E-03	1.98	1.0100E-02	2.04	0.5
1/32	7.7186E-04	1.96	2.5000E-03	2.01	0.5
1/64	1.9435E-04	1.99	6.2402E-04	2.00	0.5

Table 5.19: Errors and convergence rates of Algorithm 3.1 (IIPG) with dual partition parameters $a = (1 - 1/\sqrt{3})/2, b = (6 + \sqrt{3} - \sqrt{21 + 6\sqrt{3}})/9$ for Example 5.2.

h	$\|u - u_h\|_0$	Rate	$\|\|\|u - u_h\|\|\|$	Rate	α
1/4	2.0000E-03		1.4650E-01		16
1/8	2.0347E-04	3.30	3.7400E-02	1.97	64
1/16	2.2902E-05	3.15	9.4000E-03	1.99	256
1/32	2.7657E-06	3.05	2.4000E-03	1.97	1024
1/64	3.4232E-07	3.01	5.9055E-04	2.02	4096

Table 5.20: Errors and convergence rates of Algorithm 3.1 (IIPG) with dual partition parameters $a = (1 - 1/\sqrt{3})/2, b = (6 + \sqrt{3} - \sqrt{21 + 6\sqrt{3}})/9$ for Example 5.2.

h	$\|u - u_h\|_0$	Rate	$\|\|\|u - u_h\|\|\|$	Rate	α
1/4	3.2000E-03		1.4560E-01		10
1/8	7.9872E-04	2.00	3.6300E-02	2.00	10
1/16	2.0348E-04	1.97	9.0000E-03	2.01	10
1/32	5.1564E-05	1.98	2.3000E-03	1.97	10
1/64	1.2990E-05	1.99	5.6312E-04	2.03	10

Table 5.21: Errors and convergence rates of Algorithm 3.2 (NIPG) with dual partition parameters $a = b = (1 - 1/\sqrt{3})/2$ for Example 5.2.

h	$\|u - u_h\|_0$	Rate	$\|\|\|u - u_h\|\|\|$	Rate	α
1/4	1.1100E-02		1.3410E-01		0.1
1/8	2.8000E-03	1.99	3.1900E-02	2.07	0.1
1/16	6.9010E-04	2.02	7.8000E-03	2.03	0.1
1/32	1.7216E-04	2.00	1.9000E-03	2.04	0.1
1/64	4.2988E-05	2.00	4.7407E-04	2.00	0.1

Table 5.22: Errors and convergence rates of Algorithm 3.2 (NIPG) with dual partition parameters $a = b = (1 - 1/\sqrt{3})/2$ for Example 5.2.

h	$\|u - u_h\|_0$	Rate	$\|\|\|u - u_h\|\|\|$	Rate	α
1/4	1.1300E-02		1.3490E-01		0.001
1/8	2.8000E-03	2.01	3.2000E-02	2.08	0.001
1/16	6.9416E-04	2.01	7.8000E-03	2.04	0.001
1/32	1.7283E-04	2.01	1.9000E-03	2.04	0.001
1/64	4.3113E-05	2.00	4.7605E-04	2.00	0.001

Table 5.23: Errors and convergence rates of Algorithm 3.2 (NIPG) with dual partition parameters $a = b = (1 - 1/\sqrt{3})/2$ for Example 5.2.

h	$\|u - u_h\|_0$	Rate	$\|\|\|u - u_h\|\|\|$	Rate	α
1/4	4.5000E-03		1.4260E-01		10
1/8	1.2000E-03	1.91	3.5300E-02	2.01	10
1/16	3.0106E-04	1.99	8.8000E-03	2.00	10
1/32	7.6632E-05	1.97	2.2000E-03	2.00	10
1/64	1.9338E-05	1.99	5.4616E-04	2.01	10

Table 5.24: Errors and convergence rates of Algorithm 3.2 (NIPG) with dual partition parameters $a = (1 - 1/\sqrt{3})/2, b = (6 + \sqrt{3} - \sqrt{21 + 6\sqrt{3}})/9$ for Example 5.2.

h	$\|u - u_h\|_0$	Rate	$\|\|\|u - u_h\|\|\|$	Rate	α
1/4	3.0000E-03		1.4490E-01		16
1/8	2.7813E-04	3.43	3.7300E-02	1.96	64
1/16	2.6347E-05	3.40	9.4000E-03	1.99	256
1/32	2.8911E-06	3.19	2.4000E-03	1.97	1024
1/64	3.4634E-07	3.06	5.9055E-04	2.02	4096

Table 5.25: Errors and convergence rates of Algorithm 3.2 (NIPG) with dual partition parameters $a = (1 - 1/\sqrt{3})/2, b = (6 + \sqrt{3} - \sqrt{21 + 6\sqrt{3}})/9$ for Example 5.2.

h	$\|u - u_h\|_0$	Rate	$\|\|\|u - u_h\|\|\|$	Rate	α
1/4	4.0000E-03		1.4210E-01		10
1/8	1.0000E-03	2.00	3.5200E-02	2.01	10
1/16	2.7139E-04	1.88	8.7000E-03	2.02	10
1/32	6.9240E-05	1.97	2.2000E-03	1.98	10
1/64	1.7494E-05	1.98	5.4315E-04	2.02	10

Table 5.26: Errors and convergence rates of Algorithm 3.3 (SIPG) with dual partition parameters $a = b = (1 - 1/\sqrt{3})/2$ for Example 5.2.

h	$\|u - u_h\|_0$	Rate	$\|\|\|u - u_h\|\|\|$	Rate	α
1/4	1.3000E-03		1.5380E-01		10
1/8	1.9975E-04	2.70	3.8200E-02	2.01	10
1/16	4.1220E-05	2.28	9.5000E-03	2.01	10
1/32	9.7206E-06	2.08	2.4000E-03	1.98	10
1/64	2.3928E-06	2.02	5.9443E-04	2.01	10

Table 5.27: Errors and convergence rates of Algorithm 3.3 (SIPG) with dual partition parameters $a = b = (1 - 1/\sqrt{3})/2$ for Example 5.2.

h	$\|u - u_h\|_0$	Rate	$\|\|\|u - u_h\|\|\|$	Rate	α
1/4	1.3000E-03		1.5000E-01		16
1/8	2.1616E-04	2.59	3.7500E-02	2.00	64
1/16	3.9630E-05	2.45	9.4000E-03	2.00	256
1/32	8.6678E-06	2.19	2.4000E-03	1.97	1024
1/64	2.0802E-06	2.06	5.9058E-04	2.02	4096

Table 5.28: Errors and convergence rates of Algorithm 3.3 (SIPG) with dual partition parameters $a = (1 - 1/\sqrt{3})/2, b = (6 + \sqrt{3} - \sqrt{21 + 6\sqrt{3}})/9$ for Example 5.2.

h	$\|u - u_h\|_0$	Rate	$\|\|\|u - u_h\|\|\|$	Rate	α
1/4	1.0000E-03		1.5340E-01		10
1/8	1.2480E-04	3.00	3.8100E-02	2.01	10
1/16	1.5686E-05	2.99	9.5000E-03	2.00	10
1/32	2.1705E-06	2.85	2.4000E-03	1.98	10
1/64	3.6390E-07	2.58	5.9214E-04	2.02	10

Table 5.29: Errors and convergence rates of Algorithm 3.3 (SIPG) with dual partition parameters $a = (1 - 1/\sqrt{3})/2, b = (6 + \sqrt{3} - \sqrt{21 + 6\sqrt{3}})/9$ for Example 5.2.

h	$\|u - u_h\|_0$	Rate	$\|\|\|u - u_h\|\|\|$	Rate	α
1/4	1.2000E-03		1.4970E-01		16
1/8	1.6501E-04	2.86	3.7400E-02	2.00	64
1/16	2.1504E-05	2.94	9.4000E-03	1.99	256
1/32	2.7193E-06	2.98	2.4000E-03	1.97	1024
1/64	3.4094E-07	3.00	5.9055E-04	2.02	4096

Table 5.30: Errors and convergence rates of Algorithm 3.3 (SIPG) with dual partition parameters $a = (1 - 1/\sqrt{3})/2, b = (6 + \sqrt{3} - \sqrt{21 + 6\sqrt{3}})/9$ for Example 5.2.

h	$\|u - u_h\|_0$	Rate	$\|\|\|u - u_h\|\|\|$	Rate	α
1/4	1.4000E-03		1.4970E-01		120
1/8	1.7173E-04	3.03	3.7600E-02	1.99	240
1/16	2.1654E-05	2.99	9.4000E-03	2.00	480
1/32	2.7186E-06	2.99	2.4000E-03	1.97	960
1/64	3.4057E-07	3.00	5.9043E-04	2.02	1920

method in this paper preserves both the local conservation properties of the finite volume element method and the flexibility and accuracy of the DG method.

It is worth noting that the L^2-norm error estimate of quadratic FVM is affected by dual partition. The authors of reference [21] studied the L^2-norm error analysis of higher-order continuous finite volume method for linear elliptic problems. It is shown that when the dual parameters defined in (2.2) are respectively valued as $a = (1 - 1/\sqrt{3})/2, b = (6 + \sqrt{3} - \sqrt{21 + 6\sqrt{3}})/9$, the error in L^2-norm of the corresponding quadratic FVM approximation solution can achieve the optimal convergence rate.

In this paper, the error of the quadratic discontinuous FVM scheme with parameters $a = (1-1/\sqrt{3})/2, b = (6+\sqrt{3}-\sqrt{21+6\sqrt{3}})/9$ for solving the elliptic problem is also calculated, and the specific error data for Example 5.1 are shown in Tables 5.4-5.5, Tables 5.9-5.10, Tables 5.13-5.15, and for Example 5.2 are shown in Tables 5.19-5.20, Tables 5.24-5.25, Tables 5.28-5.30, respectively. Figs. 5.1-5.3, and Figs. 5.4-5.6 plot the error convergence rates for numerical solutions obtained by the three DFVM schemes under different penalty parameters and dual parameters for Examples 5.1 and 5.2, respectively.

It can be found from the data in these tables and figures that when the problem is solved on the dual partition constructed by the above parameters and the penalty parameter α is $1/h^2$ for three schemes or α is $30/h$ for Algorithm 3.3, the calculation results satisfy the L^2-norm error order of the approximate solution is third-order. However, the L^2-norm errors of three quadratic discontinuous finite volume solution both fails to achieve optimal convergence rate when the penalty parameter α is set at 10. This indicates that the L^2 estimates for quadratic DFVM solution is also related to the penalty parameter.

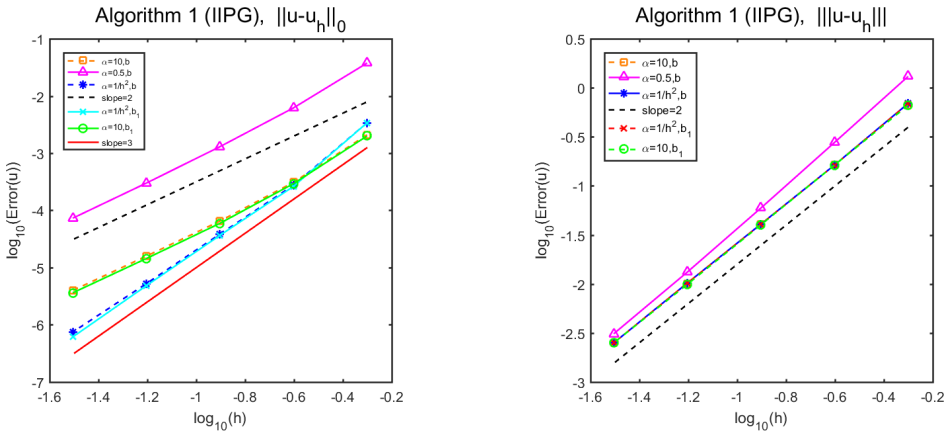

Fig. 5.1. The convergence rates of the Algorithm 3.1 (IIPG) with the different dual partition $a = b = (1-1/\sqrt{3})/2, b_1 = (6+\sqrt{3}-\sqrt{21+6\sqrt{3}})/9$ and penalty parameter α for Example 5.1.

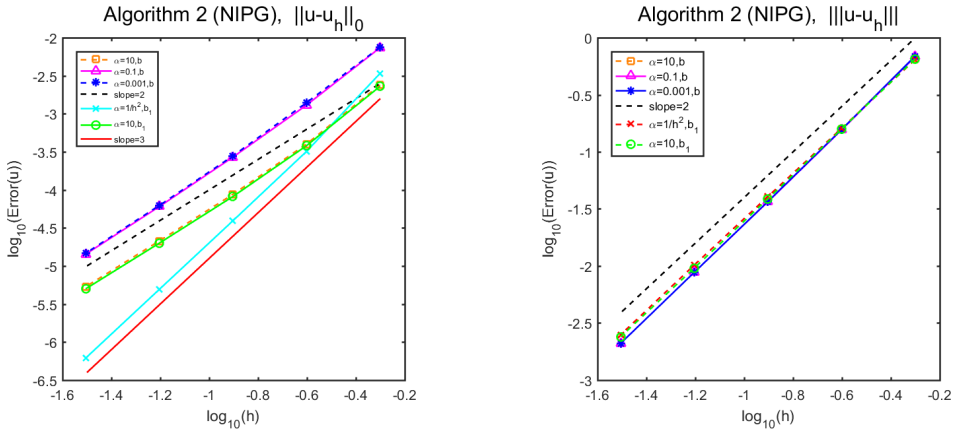

Fig. 5.2. The convergence rates of the Algorithm 3.2 (NIPG) with the different dual partition $a = b = (1-1/\sqrt{3})/2, b_1 = (6+\sqrt{3}-\sqrt{21+6\sqrt{3}})/9$ and penalty parameter α for Example 5.1.

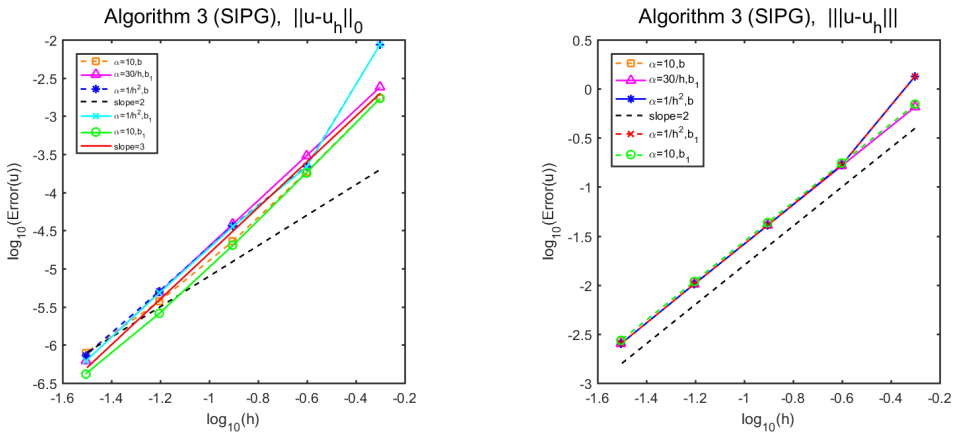

Fig. 5.3. The convergence rates of the Algorithm 3.3 (SIPG) with the different dual partition $a = b = (1 - 1/\sqrt{3})/2, b_1 = (6 + \sqrt{3} - \sqrt{21 + 6\sqrt{3}})/9$ and penalty parameter α for Example 5.1.

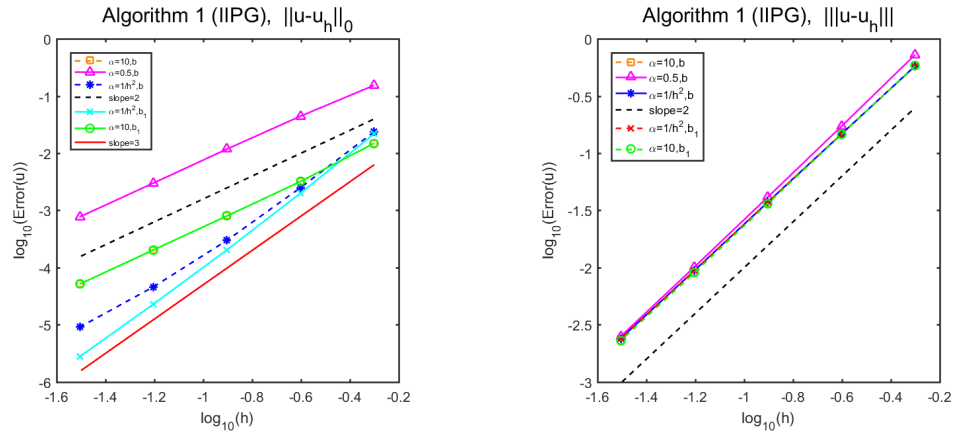

Fig. 5.4. The convergence rates of the Algorithm 3.1 (IIPG) with the different dual partition $a = b = (1 - 1/\sqrt{3})/2, b_1 = (6 + \sqrt{3} - \sqrt{21 + 6\sqrt{3}})/9$ and penalty parameter α for Example 5.2.

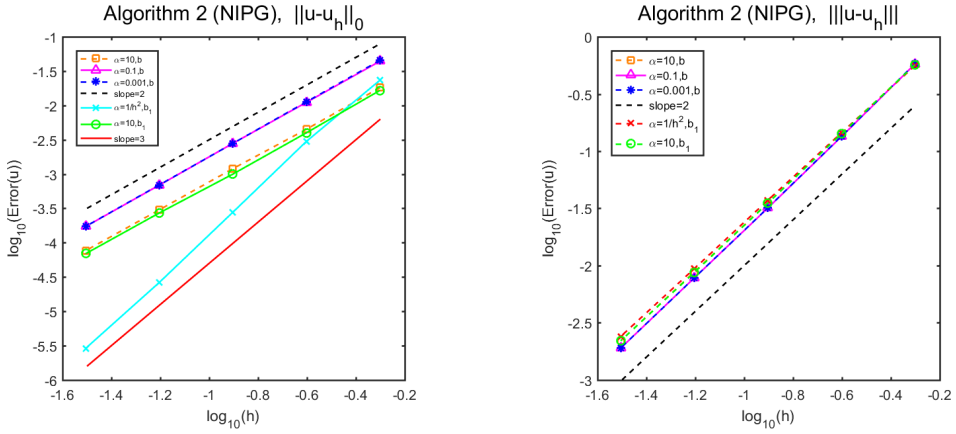

Fig. 5.5. The convergence rates of the Algorithm 3.2 (NIPG) with the different dual partition $a = b = (1 - 1/\sqrt{3})/2, b_1 = (6 + \sqrt{3} - \sqrt{21 + 6\sqrt{3}})/9$ and penalty parameter α for Example 5.2.

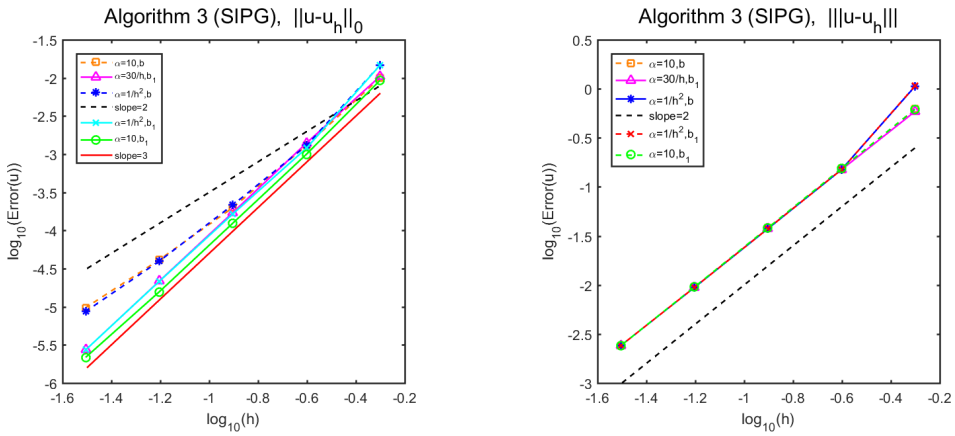

Fig. 5.6. The convergence rates of the Algorithm 3.3 (SIPG) with the different dual partition $a = b = (1 - 1/\sqrt{3})/2, b_1 = (6 + \sqrt{3} - \sqrt{21 + 6\sqrt{3}})/9$ and penalty parameter α for Example 5.2.

6. Conclusions

For the second-order elliptic problem, we propose the quadratic discontinuous finite volume element algorithms with incomplete symmetric, nonsymmetric, and symmetric internal penalty types, respectively, which not only can achieve the second-order accuracy as the discontinuous Galerkin methods, but also possess local conservation of physical quantities within the control volume. Additionally, the convergence analysis of three algorithms is also provided. Numerical experiments are conducted to validate the performance of the three DFVM algorithms, confirm the theoretical results, and investigate the effects of different dual partitions and penalty parameters on the DFVM algorithms. In future work, we will further explore the relationship between the optimal order L^2 error estimation and the penalty parameter in the theoretical aspect of higher-order DFVMs.

Acknowledgements. The authors would like to sincerely thank the reviewers for their valuable suggestions and constructive feedback, which will go a long way in improving the quality of the paper. The authors would like to thank Professor Rui Li for his valuable guidance and suggestions.

This work is supported by the National Natural Science Foundation of China (Grant No. 12131014), and by the Key Program of Natural Science Foundation of Ningxia (Grant No. 2022AAC02004).

References

[1] D.N. Arnold, An interior penalty finite element method with discontinuous elements, *SIAM J. Numer. Anal.*, **19**:4 (1982), 742–760.

[2] D.N. Arnold, F. Brezzi, B. Cockburn, and L.D. Marini, Unified analysis of discontinuous Galerkin methods for elliptic problems, *SIAM J. Numer. Anal.*, **39**:5 (2002), 1749–1779.

[3] I. Babuška, The finite element method with penalty, *Math. Comp.*, **27**:122 (1973), 221–228.

[4] I. Babuška and M. Zlámal, Nonconforming elements in the finite element method with penalty, *SIAM J. Numer. Anal.*, **10**:5 (1973), 863–875.

[5] C.E. Baumann and J.T. Oden, A discontinuous *hp* finite element method for convection-diffusion problems, *Comput. Methods Appl. Mech. Engrg.*, **175**:3-4 (1999), 311–341.

[6] L. Chen, A new class of high order finite volume methods for second order elliptic equations, *SIAM J. Numer. Anal.*, **47**:6 (2010), 4021–4043.

[7] Z. Chen, J. Wu, and Y. Xu, Higher-order finite volume methods for elliptic boundary value problems, *Adv. Comput. Math.*, **37**:2 (2012), 191–253.

[8] Z. Chen, Y. Xu, and Y. Zhang, Higher-order finite volume methods II: Inf-sup condition and uniform local ellipticity, *J. Comput. Appl. Math.*, **265** (2014), 96–109.

[9] Z. Chen, Y. Xu, and Y. Zhang, A construction of higher-order finite volume methods, *Math. Comp.*, **84**:292 (2015), 599–628.

[10] S. Chou, Analysis and convergence of a covolume method for the generalized Stokes problem, *Math. Comp.*, **66**:217 (1997), 85–104.

[11] S.-H. Chou and X. Ye, Unified analysis of finite volume methods for second order elliptic problems, *SIAM J. Numer. Anal.*, **45**:4 (2007), 1639–1653.

[12] B. Cockburn and C.W. Shu, The local discontinuous Galerkin method for time-dependent convection-diffusion systems, *SIAM J. Numer. Anal.*, **35**:6 (1998), 2440–2463.

[13] R. Eymard, R. Herbin, and J. C. Latché, On a stabilized colocated finite volume scheme for the Stokes problem, *ESAIM Math. Model. Numer. Anal.*, **40**:3 (2006), 501–527.

[14] R. Li, Y. Gao, J. Chen, L. Zhang, X. He, and Z. Chen, Discontinuous finite volume element method for a coupled Navier-Stokes-Cahn-Hilliard phase field model, *Adv. Comput. Math.*, **46** (2020), 25.

[15] R. Li, Y. Gao, J. Li, and Z. Chen, Discontinuous finite volume element method for a coupled non-stationary Stokes-Darcy problem, *J. Sci. Comput.*, **74**:2 (2018), 693–727.

[16] Y. Lou and H. Rui, A quadratic discontinuous finite volume element scheme for Stokes problems, *J. Sci. Comput.*, **99**:2 (2024), 44.

[17] W.H. Reed and T.R. Hill, *Triangular Mesh Methods for the Neutron Transport Equation*, Technical Report, Los Alamos Scientific Laboratory, University of California, 1973.

[18] H. Rui, Symmetric modified finite volume element methods for self-adjoint elliptic and parabolic problems, *J. Comput. Appl. Math.*, **146**:2 (2002), 373–386.

[19] H. Rui, Analysis on a finite volume element method for Stokes problems, *Acta Math. Appl. Sin.*, **21**:3 (2005), 359–372.

[20] G. Wang, Y. He, and R. Li, Discontinuous finite volume methods for the stationary Stokes-Darcy problem, *Internat. J. Numer. Methods Engrg.*, **107**:5 (2016), 395–418.

[21] X. Wang and Y. Li, L^2 error estimates for high order finite volume methods on triangular meshes, *SIAM J. Numer. Anal.*, **54**:5 (2016), 2729–2749.

[22] M.F. Wheeler, An elliptic collocation-finite element method with interior penalties, *SIAM J. Numer. Anal.*, **15**:1 (1978), 152–161.

[23] J. Xu and Q. Zou, Analysis of linear and quadratic simplicial finite volume methods for elliptic equations, *Numer. Math.*, **111**:3 (2009), 469–492.

[24] H. Yang and Y. Li, The mixed finite volume method for Stokes problem based on mini element pair, *Int. J. Numer. Anal. Model.*, **20**:1 (2023), 134–151.

[25] X. Ye, On the relationship between finite volume and finite element methods applied to the Stokes equations, *Numer. Methods Partial Differential Equations*, **17**:5 (2001), 440–453.

[26] X. Ye, A new discontinuous finite volume method for elliptic problems, *SIAM J. Numer. Anal.*, **42**:3 (2004), 1062–1072.

[27] J. Zhang, A family of quadratic finite volume method for solving the Stokes equation, *Comput. Math. Appl.*, **117** (2022), 155–186.

[28] T. Zhang and L. Tang, A stabilized finite volume method for Stokes equations using the lowest order $P_1 - P_0$ element pair, *Adv. Comput. Math.*, **41**:4 (2015), 781–798.

[29] Q. Zou, An unconditionally stable quadratic finite volume scheme over triangular meshes for elliptic equations, *J. Sci. Comput.*, **70**:1 (2017), 112–124.